The approach of the two phthalocyanine units in one naphthalene or anthracene binuclear species may be closer, therefore, than in the corresponding binuclear porphyrin.

Table II summarizes the splitting energies observed for a range of phthalocyanine species. Although several factors affect the size of K_c,[27a] electrostatic interactions must play an important role. Particularly in the syn form, the two phthalocyanine planes are in close proximity. However the distance between the phthalocyanine units in the 1,8-naphthalene species has been estimated as at least 4.3 Å (section i), compared with the van der Waals contact (3.6 Å) (or shorter in some silicon-bridged phthalocyanine species, 3.3 Å).[9c,10] The mixed-valence splitting energies for oxidation of the silicon phthalocyanine RSiPc-O-PcSiR binuclear species are on the order of 0.4-0.5 V[10] and therefore rather larger than those reported here. This value is indicative of that to be expected at close contact when the rings are well aligned.

The mixed-valence splitting energies for reduction of the silicon binuclear species are about 0.4 V[10] and likely provide an upper limit for sideways interactions of the π clouds in the reduced ring species. This splitting is comparable or less than the $Co^{II}Co^{I}$ splitting data reported here. These larger $Co^{II}Co^{I}$ values are likely a consequence of the interaction between the cobalt d_{z^2} orbitals, which point directly toward one another along the inter-ring axis. While magnetic studies could provide useful information concerning the electronic structures of both the $[Co^{II}TrNPcCo^{II}TrNPc]$ and $[Co^{II}TrNPcCo^{I}TrNPc]^-$ species of complexes, it is premature to attempt such measurements until a means has been found to separate the syn and anti isomers.

Comparison of the "corrected" exciton data (Table V) of these anthracene and naphthalene species with those for the flexible clamshell EtMeO(5) species does show that the former species have greater exciton splitting and this is consistent with the increased electrochemical mixed-valence splitting.

The lack of mixed-valence oxidation products for the cobalt flexible clamshell species may reflect the formation of six-coordinate Co(III) species when a donor solvent or electrolyte anion is present, thus forcing the two rings apart. This may also occur with $Co^{II}Pc(-1)$ species since formation of the Pc(-1) oxidation state will increase the Lewis acidity of the cobalt atom.

Stepwise oxidation of the two rings in a binuclear phthalocyanine species places a positive charge on one ring, which will then attract the electron density on the other ring, favoring formation of a mixed-valence delocalized oxidation species. On the other hand, there is no firm evidence for the formation of mixed-valence anion-radical species in the current series of binuclear complexes, albeit that the DCB electrochemical data are ambiguous in this respect. In this redox level, there is an added electron making one ring negatively charged and causing repulsion of the other ring.

Thus mixed-valence behavior has been established for the following classes of phthalocyanine compounds.

Pc(-1)Pc(-2) is observed with cobalt and in main-group species such as silicon and zinc. Although not fully investigated here, it is likely that mixed-valence Pc(-1)Pc(-2) species containing either cobalt(II) or cobalt(III) can be derived by appropriate choice of solvent or medium.

$Co^{II}Co^{I}$ is observed in inflexible binuclear cobalt phthalocyanines; this mixed valence species has significant stability due to delocalization of the charge.

$Co^{III}Co^{II}$ is observed in inflexible binuclear phthalocyanines.

Pc(-2)Pc(-3) is observed in rigid main-group M-bridge-M species such as RSiPc-O-PcSR, but less readily obtained in flexible binuclear species.

There is every reason to expect that the above observations are fairly general and that most transition-metal ions would yield mixed-valence complexes in pillared phthalocyanine species. This study provides the foundation for future studies in mixed-valence phthalocyanine chemistry. It is possible to predict with some certainly the situations that should give rise to mixed-valence phthalocyanine chemistry and estimate the energetics thereof and hence to use this capability in a design sense for technological application.

Acknowledgment. We are indebted to the Natural Sciences and Engineering Research Council (Ottawa) and the Office of Naval Research (Washington, DC) for financial assistance. We thank Union Carbide (Parma) for the gift of highly oriented pyrolytic graphite.

Contribution from the Departments of Chemistry, Drexel University, Philadelphia, Pennsylvania 19104, University of Virginia, Charlottesville, Virginia 22901, and Memorial University of Newfoundland, St. John's, Newfoundland, Canada A1B 3X7

Analogues for the Specific Iron-Binding Site in the Transferrins: Molecular Structure of a Ternary Iron(III) Model Complex and Spectroscopic, Redox, and Reactivity Properties of Related Compounds

Michael R. McDevitt,[1a] Anthony W. Addison,*[,1a] Ekkehard Sinn,*[,1b] and Laurence K. Thompson[1c]

Received August 1, 1989

Small-molecule analogues of the specific iron-binding site of the iron tyrosinate protein lactoferrin have been prepared and characterized. The single-crystal X-ray structure of an *N*-methylimidazole adduct of one of these complexes, (2-(benzimidazol-2-ylmethyl)phenolato)(2-oxo-3-methylbenzoato)bis(*N*-methylimidazole)iron(III), has been determined by standard procedures and refined by least-squares methods to a conventional *R* factor of 0.061. The purple crystals belong to the orthorhombic space group *Pbca* with $Z = 8$ and unit cell dimensions $a = 17.470$ (5) Å, $b = 17.030$ (6) Å, and $c = 18.910$ (7) Å. The iron(III) complex has a pseudooctahedral N_3O_3 donor set, utilizing bidentate ligands to provide phenolate, benzimidazole, and carboxylate coordination to mimic respectively the known tyrosinate, histidine, and aspartate protein side chains. The model complexes, which do not include any severe steric constraints, mimic several features of the transferrins: (i) tyrosinate-to-iron(III) charge-transfer band wavelength and molar absorptivity; (ii) reactivity with cyanide to produce a low-spin iron(III) adduct; and (iii) a quite negative value of $E_{1/2}$. The relationship between these analogues and the active sites of the transferrins is discussed in light of these results.

Introduction

The transferrins (serum transferrin, lactoferrin, and ovotransferrin) are an important subclass of iron(III) tyrosinate proteins[2] that reversibly bind 2 mol of iron(III) cooperatively with 2 mol of carbonate or bicarbonate.[3] Inorganic coordination complexes designed to model the iron active site in transferrin[4-8]

(1) (a) Drexel University. (b) University of Virginia. (c) Memorial University of Newfoundland.

(2) Que, L., Jr. *Coord. Chem. Rev.* **1983**, *50*, 73.
(3) Chasteen, N. D. *Coord. Chem. Rev.* **1977**, *22*, 1.

0020-1669/90/1329-3425$02.50/0

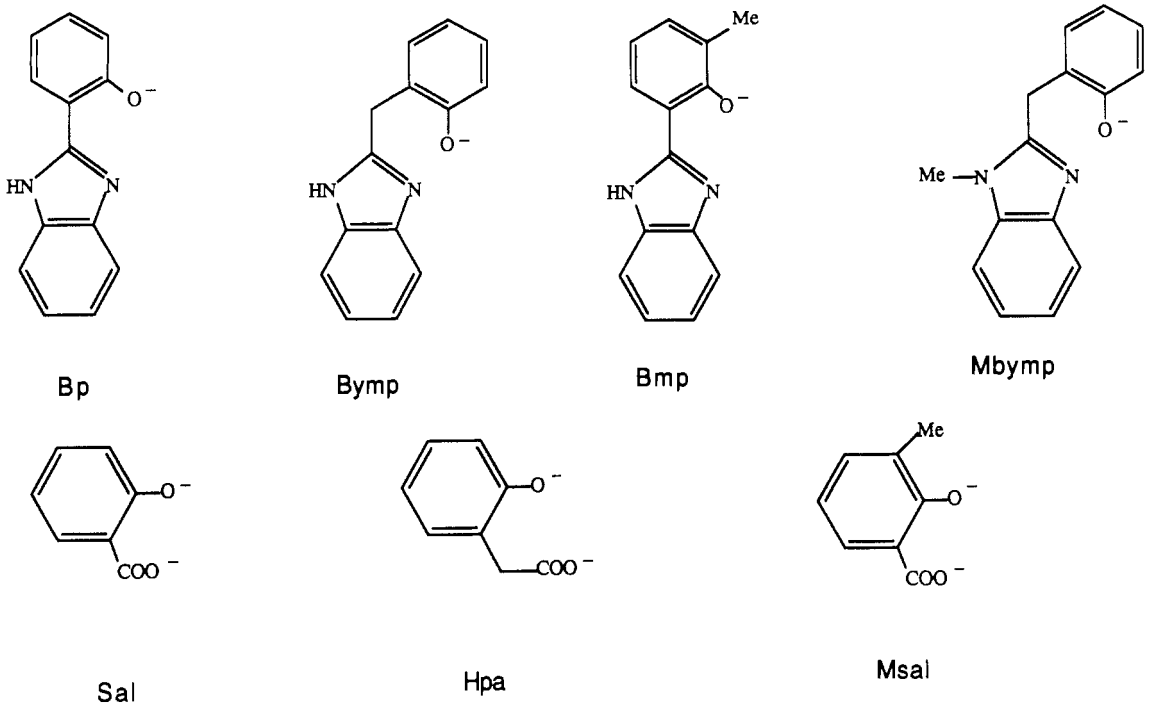

Figure 1. The ligands utilized.

Table I. Compositions of the Iron(III) Complexes

			Anal., %					
			calcd			found		
compd	compn	empirical form	C	H	N	C	H	N
1	$Fe(Bp)(Sal)\cdot 4.25H_2O$	$C_{20}H_{13}FeN_2O_4\cdot 4.25H_2O$	50.3	4.54	5.86	50.0	3.49	5.54
2	$Fe(Bmp)(Sal)\cdot 1.3H_2O\cdot EtOH$	$C_{21}H_{15}FeN_2O_4\cdot 1.3H_2O\cdot EtOH$	56.9	4.91	5.77	57.0	4.39	5.61
3	$Fe(Bmp)(Hpa)\cdot 2.5H_2O$	$C_{22}H_{17}FeN_2O_4\cdot 2.5H_2O$	55.7	4.68	5.91	56.0	4.37	5.70
4	$Fe(Bymp)(Sal)\cdot 2.5H_2O$	$C_{21}H_{15}FeN_2O_4\cdot 2.5H_2O$	54.8	4.38	6.09	55.2	4.28	5.69
5	$Fe(Bymp)(Hpa)\cdot 3H_2O$	$C_{22}H_{17}FeN_2O_4\cdot 3H_2O$	54.7	4.80	5.80	54.3	4.33	5.42
6	$Fe(Bp)(Hpa)\cdot 2H_2O$	$C_{21}H_{15}FeN_2O_4\cdot 2H_2O$	55.9	4.24	6.21	55.7	4.05	5.93
7	$Fe(Bp)(Msal)\cdot 2.5H_2O$	$C_{21}H_{15}FeN_2O_4\cdot 2.5H_2O$	54.8	4.38	6.09	54.6	3.86	5.90
8	$Fe(Bmp)(Msal)\cdot 2H_2O$	$C_{22}H_{17}FeN_2O_4\cdot 2H_2O$	56.8	4.55	6.02	56.5	4.27	5.72
9	$Fe(Bymp)(Msal)\cdot 3.5H_2O$	$C_{22}H_{17}FeN_2O_4\cdot 3.5H_2O$	53.7	4.91	5.69	53.4	4.19	5.36
10	$Fe(Mbymp)(Sal)\cdot 3.25H_2O$	$C_{22}H_{17}FeN_2O_4\cdot 3.25H_2O$	54.2	4.86	5.74	54.2	4.31	5.72
11	$Fe(Mbymp)(Hpa)\cdot 2.66H_2O$	$C_{23}H_{19}FeN_2O_4\cdot 2.66H_2O$	56.2	4.99	5.70	56.1	4.61	5.36
$9(Mim)_2$	$Fe(Bymp)(Msal)(Mim)_2$	$C_{30}H_{29}FeN_6O_4$	60.7	4.93	14.2	60.1	5.02	14.9

had not been able to resolve unequivocally the actual ligand ensemble in the protein on the basis of spectroscopic comparisons. However, the recent crystallographic structure determinations of human lactoferrin (Fe_2Lf)[9] and rabbit serum transferrin (Fe_2Tf) reveal that the protein molecules entail two iron-binding domains, one C-terminal and the other N-terminal. The lactoferrin structure shows directly that the amino acids (one histidine, two *cis*-tyrosinates, and an aspartate) ligating the iron(III) ion occupy four coordination sites with two additional cis positions open for the coordination of the (bi)carbonate anion. The uptake of both iron(III) atoms by transferrin is well understood (K is approximately 10^{20} at pH 7.4); however, the mechanism of release is open to speculation. Some have suggested[10] that reduction to iron(II) might be a requisite for iron release on the basis of the substantially smaller binding constant of the protein for iron(II) (K is approximately $10^{7.4}$).[11]

The aim of this study was to prepare molecular analogues of lactoferrin, incorporating ligands that mimic the four established amino acid residues, which provide further information pertinent to an understanding of the spectroscopy, function, and reactivity of the active site. This appears to be the first time that a nonconjugated, non Schiff base ligand (Bymp/Mbymp, Figure 1) incorporating both imidazole-derived nitrogen and phenolate oxygen has been used to model such Fe–protein active sites. Spectroscopic, magnetic, and electrochemical data are presented for a series of systematically modified model compounds, as well as the X-ray crystal structure of the *N*-methylimidazole adduct of one of these compounds. The relevance of the model complexes is discussed in light of these results in order to provide information concerning the nature of the iron coordination chemistry in the protein.

(4) Carrano, C. J.; Spartalian, K.; Rao, G. V. N. A.; Pecoraro, V. L.; Sundaralingam, M. *J. Am. Chem. Soc.* **1985**, *107*, 1651.
(5) Ainscough, E. W.; Brodie, A. M.; Plowman, J. E.; Brown, K. L.; Addison, A. W.; Gainsford, A. R. *Inorg. Chem.* **1980**, *19*, 3655.
(6) Casella, L.; Gullotti, M.; Pintar, A.; Messori, L.; Rockenbauer, A.; Gyor, M. *Inorg. Chem.* **1987**, *26*, 1031.
(7) Pyrz, J. W.; Roe, A. L.; Stern, L. J.; Que, L., Jr. *J. Am. Chem. Soc.* **1985**, *107*, 641.
(8) Gaber, B. P.; Miskowski, V.; Spiro, T. G. *J. Am. Chem. Soc.* **1974**, *96*, 6868.
(9) (a) Anderson, B. F.; Baker, H. M.; Dodson, E. J.; Norris, G. E.; Rumball, S. V.; Waters, J. M.; Baker, E. N. *Proc. Natl. Acad. Sci. U.S.A.* **1987**, *84*, 1769. (b) Anderson, B. F.; Baker, H. M.; Haridas, M.; Norris, G. E.; Rumball, S. V.; Smith, C. A.; Baker, E. N. *Abstracts*, XXVIIth International Conference on Coordination Chemistry, Brisbane, Australia, 1989; S20. (c) Bailey, S.; Evans, R. W.; Garratt, R. C.; Gorinsky, B.; Hasnain, S.; Horsburgh, C.; Jhoti, H.; Lindley, P. F.; Mydin, A.; Sarra, R.; Watson, J. L. *Biochemistry* **1988**, *27*, 5804. Note added in proof: the Fe–Fe coupling free energy in transferrin is ca. 3 kJ mol^{-1}: Bali, P. K.; Harris, W. R. *J. Am. Chem. Soc.* **1989**, *111*, 4457.
(10) Kretchmar, S. A.; Reyes, Z. E.; Raymond, K. N. *Biochim. Biophys. Acta* **1988**, *956*, 85.
(11) Harris, W. R. *Biochemistry* **1983**, *22*, 3920.

Table II. Crystallographic Data for Fe(Bymp)(Msal)(Mim)$_2$

formula	$FeC_{30}H_{29}N_6O_4$	Z	8
fw	593.44	ρ_{calcd}, g cm^{-3}	1.40
space group	*Pbca* (No. 61)	μ(Mo Kα), cm^{-1}	6.01
a, Å	17.470 (5)	R	0.061
b, Å	17.030 (6)	R_w	0.077
c, Å	18.910 (7)	T, °C	20
V, Å^3	5626 (6)	λ(Mo Kα, graphite-monochromated), Å	0.71069

Experimental Section

Synthesis of the Ligands. Figure 1 identifies the ligands in the ionic forms utilized in the synthetic preparations and gives the abbreviations used in this paper. 2-Hydroxybenzoic acid (salicylic acid, $SalH_2$), (*o*-hydroxyphenyl)acetic acid ($HpaH_2$), and 2-hydroxy-3-methylbenzoic acid (3-methylsalicylic acid, $MsalH_2$) were purchased from Aldrich and used without further purification. 2-(Benzimidazol-2-yl)phenol (BpH) and 2-(benzimidazol-2-yl)-3-methylphenol (BmpH) were prepared by the method of Addison and Burke.[12] 2-(Benzimidazol-2-ylmethyl)phenol (BympH) and 2-(*N*-methylbenzimidazol-2-ylmethyl)phenol (MbympH) were prepared by the method of Wahlgren and Addision.[13]

Preparation of the Complexes. Table I presents the analytical results for the iron complexes prepared for this work and describes the ligand and solvent composition of the ternary complexes. The quality of the analytical data is typical of compounds of this class.[6] The following synthetic procedure for complex **1** describes the general method of preparation of all of the ternary complexes used in this study. The microcrystalline complexes are generally deep red-purple.

Preparation of Fe(Bp)(Sal)·4.25H$_2$O (1). To a solution of 0.77 g (1.5 mmol) of $Fe(ClO_4)_3{\cdot}9H_2O$[14] (G. F. Smith Chemical Co.) in 5 mL of absolute ethanol was added a solution of 0.21 g (1.5 mmol) of $SalH_2$ (ionized with 2 equiv of KOH) in 30 mL of absolute ethanol followed by 0.32 g (1.5 mmol) of BpH (ionized with 1 equiv of KOH) in 30 mL of absolute ethanol. This solution was stirred for 1 h, after which time solid $KClO_4$ was filtered off, and the purple filtrate was rotary-evaporated to dryness. The solid residue was dissolved in acetone, the solution was filtered, and the filtrate was again stripped of solvent. The resulting solid was washed thoroughly with CH_2Cl_2 and dried overnight in vacuo over P_4O_{10}.

Preparation of Fe(Bymp)(Msal)(Mim)$_2$ [9-(Mim)$_2$]. To complex **9**, dissolved in CH_3CN, were added several drops of neat *N*-methylimidazole (Mim, Sigma Chemical Co.). The dark purple crystals that eventually appeared were collected by filtration, washed with anhydrous diethyl ether, recrystallized from CH_3CN, and dried in vacuo over P_4O_{10}.

Physical Measurements. Electrochemistry was performed with a three-electrode cell controlled with a PAR-173 potentiostat, a PAR-176 *i*/*E* converter, and a PAR-175 wave form generator. Potentials in nonaqueous solvent were measured with respect to the Ag^+ (0.01 M), NEt_4ClO_4 (0.1 M)/Ag electrode and may be estimated with reference to the standard hydrogen electrode (SHE) by the addition of ca. +545 mV.[15] Electrodes used for stationary-electrode cyclic voltammetry and/or rotating-disk polarography were a Beckman (rotating) platinum-risk electrode (rde, area 0.300 cm^2), an Au/Au(Hg)/Hg disk (0.289 cm^2), and a platinum-bead electrode (area 0.400 cm^2). Measurements were carried out at 25.0 ± 0.2 °C for all solutions, which were deoxygenated by bubbling purified dinitrogen (MG Industrial Gases, boiling liquid N_2). Tetraethylammonium perchlorate, TEAP (G. F. Smith, polarographic grade), was recrystallized from water and dried over P_4O_{10} in vacuo prior to being used as the supporting electrolyte. *N*,*N*-Dimethylformamide (DMF) was refluxed over and distilled off CaH_2 at reduced pressure; acetonitrile (MeCN) was refluxed over CaH_2 under dinitrogen and distilled at 1 atm. Corrections for *iR* drop were estimated from ΔE_p versus the net current ($i_{p,a} + i_{p,c}$) for a model Nernstian n = 1 process in each of the different solvents. These corrections are based on a modification of the method of Parker,[16] using the net current rather than the cathodic current to calculate values for the solution resistance. Solution density and viscosity values were as reported previously.[17]

Table III. Positional Parameters and Isotropic Equivalent Thermal Parameters for Fe(Bymp)(Msal)(Mim)$_2$

atom	x	y	z	B(eq), Å^2
Fe	0.11169 (8)	0.08004 (8)	0.16946 (8)	1.59 (7)
C1a	0.0358 (5)	0.2484 (6)	0.1068 (5)	1.5 (5)
O1a1	0.0101 (4)	0.1120 (5)	0.1341 (4)	2.8 (4)
O1a2	−0.0831 (4)	0.1866 (4)	0.0895 (4)	3.4 (4)
C2a	0.1132 (5)	0.2455 (6)	0.1198 (5)	1.1 (4)
O2a	0.1505 (4)	0.1810 (4)	0.1403 (4)	2.2 (3)
C3a	0.1604 (6)	0.3120 (6)	0.1068 (5)	1.8 (5)
C3m	0.2423 (6)	0.3079 (7)	0.1134 (7)	3.9 (7)
C4a	0.1212 (8)	0.3839 (7)	0.0890 (6)	3.8 (7)
C5a	0.0438 (7)	0.3866 (7)	0.0793 (7)	3.6 (6)
C6a	0.0022 (6)	0.3166 (6)	0.0863 (6)	3.0 (6)
C7a	−0.0148 (5)	0.1795 (6)	0.1115 (5)	1.7 (5)
C1	0.0704 (6)	−0.0932 (6)	0.1906 (6)	2.5 (6)
O1	0.0732 (4)	−0.0165 (4)	0.2042 (4)	2.4 (3)
C2	0.0528 (5)	−0.1229 (6)	0.1234 (6)	1.9 (5)
C3	0.0530 (6)	−0.2059 (6)	0.1107 (6)	2.8 (6)
C4	0.0727 (8)	−0.2548 (7)	0.1661 (7)	4.2 (7)
C5	0.0873 (7)	−0.2297 (6)	0.2312 (7)	3.8 (7)
C6	0.0837 (6)	−0.1488 (6)	0.2441 (6)	2.9 (6)
C7	0.0341 (5)	−0.0673 (6)	0.0656 (5)	1.8 (5)
C8	0.1032 (5)	−0.0281 (6)	0.0371 (5)	1.6 (5)
N9	0.1404 (4)	0.0287 (4)	0.0698 (4)	1.8 (4)
C10	0.2063 (6)	0.0407 (6)	0.0284 (5)	2.0 (5)
C11	0.2055 (6)	−0.0094 (6)	−0.0329 (5)	1.7 (5)
N12	0.1392 (5)	−0.0553 (5)	−0.0234 (4)	2.2 (4)
C13	0.2636 (6)	0.0961 (7)	0.0364 (6)	3.5 (6)
C14	0.3189 (8)	0.0992 (7)	−0.0139 (7)	6.2 (8)
C15	0.3169 (8)	0.0426 (8)	−0.0712 (8)	6.0 (8)
C16	0.2600 (6)	−0.0071 (7)	−0.0793 (5)	3.0 (6)
N1i	0.2255 (5)	0.0522 (5)	0.2063 (5)	2.3 (4)
C2i	0.2481 (6)	−0.0171 (6)	0.2273 (5)	1.8 (5)
N3i	0.3264 (5)	−0.0081 (5)	0.2520 (5)	3.4 (5)
C3im	0.3706 (7)	−0.0775 (7)	0.2762 (8)	5.5 (8)
C4i	0.3456 (6)	0.0654 (6)	0.2528 (7)	3.6 (6)
C5i	0.2883 (8)	0.1036 (7)	0.2230 (7)	4.8 (8)
N1j	0.0928 (5)	0.1259 (5)	0.2755 (4)	3.0 (5)
C2j	0.1277 (7)	0.1904 (6)	0.3005 (7)	3.9 (7)
N3j	0.1196 (5)	0.1928 (6)	0.3706 (5)	4.1 (6)
C3jm	0.145 (1)	0.254 (1)	0.4230 (7)	9 (1)
C4j	0.078 (1)	0.128 (1)	0.3873 (7)	6.8 (8)
C5j	0.0600 (8)	0.0834 (7)	0.3287 (6)	4.3 (7)
H3m1	0.2587	0.3435	0.0848	10.7
H3m2	0.2625	0.2570	0.1002	6.8
H3m3	0.2597	0.3181	0.1610	6.8
H4a	0.1522	0.4339	0.0843	6.2
H5a	0.0205	0.4356	0.0659	6.7
H6a	−0.0520	0.3181	0.0780	6.0
H3	0.0411	−0.2270	0.0637	5.2
H4	0.0728	−0.3107	0.1575	7.3
H5	0.1021	−0.2655	0.2687	6.7
H6	0.0909	−0.1295	0.2918	5.5
H71	0.0085	−0.0946	0.0292	3.6
H72	−0.0000	−0.0278	0.0844	7.1
H12	0.1224	−0.0971	−0.0529	2.7
H13	0.2658	0.1320	0.0783	6.3
H14	0.3576	0.1399	−0.0149	9.0
H15	0.3633	0.0390	−0.1022	8.3
H16	0.2572	−0.0383	−0.1217	5.7
H2i	0.2202	−0.0660	0.2245	4.8
H4i	0.3913	0.0891	0.2719	6.5
H5i	0.2898	0.1598	0.2088	7.7
H2j	0.1515	0.2295	0.2708	6.7
H4j	0.0656	0.1166	0.4360	9.2
H5j	0.0320	0.0327	0.3251	7.3

Electronic spectra were recorded on a Perkin-Elmer Lambda-3B spectrophotometer. Solvents for electronic spectroscopy were purchased from Fisher Scientific Co. and Aldrich Chemical Co. and used without further purification. Spectrophotometric titrations utilized a Gilmont 2-mL microsyringe. Electron spin resonance (ESR) spectra were recorded at 77 K and room temperature on Varian X-band spectrometers with [VO(Acac)$_2$] in benzene (Acac = acetylacetonate) and diphenylpicrylhydrazyl as standards. Elemental microanalyses were performed by Canadian Microanalytical Services Ltd. (Vancouver).

Table II contains cell dimensions and space group data for a single crystal of Fe(Bymp)(Msal)(Mim)$_2$, which were obtained by standard

(12) Addison, A. W.; Burke, P. J. *J. Heterocycl. Chem.* **1981**, *18*, 803.
(13) Wahlgren, C. G.; Addison, A. W. *J. Heterocycl. Chem.* **1989**, *26*, 541.
(14) The water content of the solid ferric perchlorate was determined by using the method described by: Flaschka, H. A. *EDTA Titrations*; Pergamon Press: New York, 1959; p 81.
(15) Addison, A. W.; Burman, S.; Wahlgren, C. G.; Rajan, O. A.; Rowe, T. M.; Sinn, E. *J. Chem. Soc., Dalton Trans.* **1987**, 2621.
(16) Parker, V. D. In *Electroanalytical Chemistry*; Bard, A. J., Ed.; Marcel Dekker: New York, 1986; Vol. 14, p 28.
(17) Addison, A. W.; Rao, T. N.; Sinn, E. *Inorg. Chem.* **1984**, *23*, 1957.

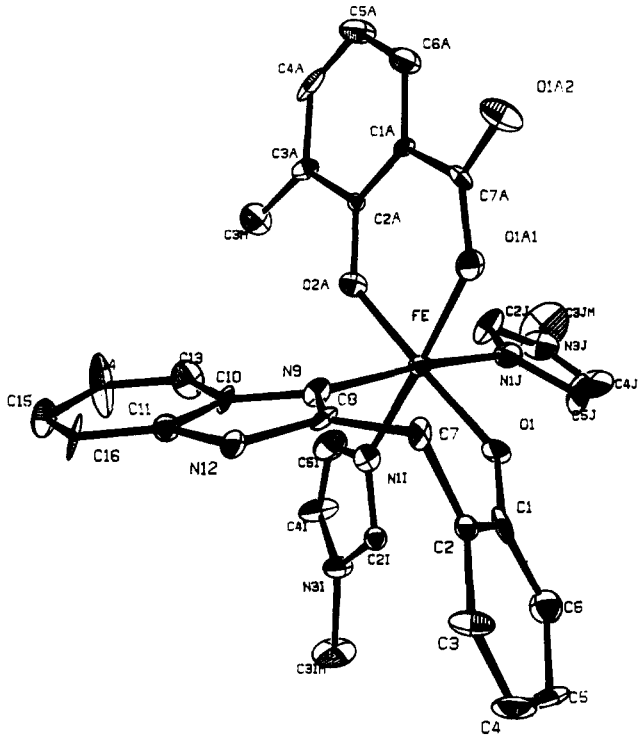

Figure 2. ORTEP diagram of the Fe(Bymp)(Msal)$(Mim)_2$ structure. Hydrogen atoms are omitted for clarity of presentation.

methods on an Enraf-Nonius CAD-4 four-circle diffractometer (Charlottesville). The θ–2θ scan technique was used, as previously described,[18] to record the intensities for all nonequivalent reflections for which $1° < 2\theta < 49.9°$. The final positional parameters for the refined atoms are listed in Table III. Standard deviations in the least significant figures in the tabulated parameters were derived from the inverse matrix in the course of least-squares refinement calculations.

Magnetic susceptibility measurements (St. John's) were obtained by using an Oxford Instuments superconducting Faraday magnetic susceptibility system with a Sartorius 4432 microbalance. A main solenoid field of 1.5 T and a gradient of 10 T m^{-1} were employed. Diamagnetic corrections for ligand susceptibilities were applied by using Pascal's constants.[19]

Results and Discussion

Ligands. The bidentate ligands afforded by the condensation of an aromatic diamine with a salicylic acid derivative provide a reasonable analogue to histidine and tyrosinate coordination via the benzimidazole and phenolate moieties. Salicylate, also a bidentate ligand, can contribute phenolate and carboxylate coordination to mimic tyrosinate and aspartate residues. These ligands are varied by the incorporation of a methylene unit in order to disrupt the conjugation between functionalities and to allow more flexibility in chelation to the metal ion.

Complexes. The ternary complexes were prepared by initially forming the iron(III) salicylate species and then adding the phenolate–benzimidazole ligand. This order of addition precludes the formation of binuclear oxo-bridged iron(III) compounds having bis(phenolate–benzimidazole) coordination.[20] The ternary complexes complete their coordination with solvent molecules. These labile solvent adducts make the isolation of a crystalline solid difficult due to their extreme solubility. The addition of *N*-methylimidazole displaces water or ethanol and coordinates to the iron(III), reducing the solubility enough to allow a crystalline solid to be obtained. Hydrogen bonding between the uncoordinated carboxylate oxygen of the salicylate ligand and the benzimidazole NH on an adjacent complex leads to the formation of a weakly bound dimeric species.

Table IV. Selected Bond Distances (Å) and Angles (deg) with Their Estimated Standard Deviations in Parentheses

Fe–O1	1.895 (5)	C8–N9	1.319 (6)
Fe–O2a	1.930 (4)	C8–N12	1.386 (7)
Fe–O1a1	1.972 (4)	N9–C10	1.408 (7)
Fe–N9	2.137 (6)	C10–C13	1.384 (9)
Fe–N1i	2.159 (5)	C10–C11	1.439 (8)
Fe–N1j	2.177 (5)	C11–C16	1.295 (8)
C1a–C6a	1.357 (8)	C11–N12	1.410 (7)
C1a–C2a	1.376 (7)	C13–C14	1.36 (1)
C1a–C7a	1.471 (8)	C14–C15	1.45 (1)
O1a1–C7a	1.302 (6)	C15–C16	1.31 (1)
O1a2–C7a	1.270 (6)	N1i–C2i	1.307 (7)
C2a–O2a	1.333 (6)	N1i–C5i	1.438 (9)
C2a–C3a	1.423 (7)	C2i–N3i	1.454 (7)
C3a–C3m	1.438 (8)	N3i–C4i	1.296 (7)
C3a–C4a	1.443 (8)	N3i–C3im	1.484 (7)
C4a–C5a	1.37 (1)	C4i–C5i	1.32 (1)
C5a–C6a	1.403 (9)	N1j–C2j	1.344 (8)
C1–O1	1.332 (6)	N1j–C5j	1.365 (8)
C1–C2	1.402 (9)	C2j–N3j	1.334 (9)
C1–C6	1.405 (8)	N3j–C4j	1.35 (1)
C2–C3	1.433 (7)	N3j–C3jm	1.51 (1)
C2–C7	1.483 (8)	C4j–C5j	1.38 (1)
C3–C4	1.38 (1)	O1a2–N12*	2.742 (8)
C4–C5	1.33 (1)	Fe–Fe*	7.984 (8)
C5–C6	1.400 (9)	N12–N12*	5.29 (1)
C7–C8	1.482 (7)	O1a2–O1a2*	7.76 (1)
O1–Fe–O2a	176.2 (3)	N1i–Fe–N1j	85.5 (2)
O1–Fe–O1a1	92.2 (2)	C7a–O1a1–Fe	131.0 (5)
O1–Fe–N9	92.0 (2)	C2a–O2a–Fe	130.1 (5)
O1–Fe–N1i	91.4 (2)	O1a2–C7a–O1a1	120.4 (8)
O1–Fe–N1j	86.4 (2)	O1a2–C7a–C1a	118.0 (8)
O2a–Fe–O1a1	88.5 (2)	O1a1–C7a–C1a	121.6 (7)
O2a–Fe–N9	91.7 (2)	C1–O1–Fe	142.8 (6)
O2a–Fe–N1i	88.0 (2)	C8–N9–Fe	126.7 (6)
O2a–Fe–N1j	89.8 (2)	C10–N9–Fe	128.5 (5)
O1a1–Fe–N9	91.4 (2)	C2i–N1i–Fe	125.1 (6)
O1a1–Fe–N1i	176.4 (2)	C5i–N1i–Fe	129.8 (7)
O1a1–Fe–N1j	94.4 (2)	C2j–N1j–Fe	123.3 (7)
N9–Fe–N1i	88.8 (2)	C5j–N1j–Fe	123.6 (7)
N9–Fe–N1j	174.0 (2)		

Description of the Structure. The complex Fe(Bymp)(Msal)$(Mim)_2$ has an N_3O_3 donor set and exhibits octahedral coordination. The structure is illustrated in Figure 2. The plane defined by atoms O2a–O1a1–N1i–O1 has a lower mean deviation than that defined by atoms O2a–N9–N1j–O1, 0.0290 versus 0.0498 Å. The dihedral angle between these two least-squares planes is 88.6°. Most of the angles (Table IV) at the iron vertex at 90 ± 2°, with the notable exceptions being the angle between the two *N*-methylimidazoles, N1i–Fe–N1j, which is 85.5°, the angle O1–Fe–N1j, which is 86.4°, and the angle O1a1–Fe–N1j, which is 94.4°. There appears to be a distinct compression of two of the ligand–iron–ligand bond angles for those ligands that comprise the O1–N1i–N1j face of the octahedron.

A comparison of the two phenolate-to-iron(III) bonds reveals that the Fe–O1 bond length is 0.035 Å shorter than the Fe–O2a bond (Table IV). The phenolate oxygen, O1, in the seven-membered chelate ring in Fe(Bymp)(Msal)$(Mim)_2$ has a rather large C1–O1–Fe angle of 142.8° compared to the C2a–O2a–Fe bond angle of 130.1° for the six-membered chelate ring. The six-membered chelate ring formed by the 3-methylsalicylate ligand with the iron(III) is essentially planar (with a mean deviation from planarity of only 0.016 Å), indicating that O2a is sp^2 hybridized and aligned so that the out-of-plane p_π orbital can interact with a half-filled d_{π^*} orbital on the iron(III) ion. In the case of O1, the hybridization either has less p character or is less ideally directed for good overlap with the iron(III) atom, as evidence by the larger C1–O1–Fe bond angle. A survey of other iron(III)–phenolate complexes[5,21–24] yields an average Fe–O–C bond angle

(18) Freyberg, D. P.; Mockler, G. M.; Sinn, E. *J. Chem. Soc., Dalton Trans.* **1976**, 447.
(19) O'Connor, C. J. In *Progress in Inorganic Chemistry*; Lippard, S. J., Ed.; John Wiley & Sons: New York, 1982; Vol. 29, p 209.
(20) Wahlgren, C. G.; Addison, A. W.; Burman, S.; Thompson, L. K.; Sinn, E. *Inorg. Chim. Acta* **1989**, *166*, 59–69.
(21) Lauffer, R. B.; Heistand, R. H., II; Que, L., Jr. *Inorg. Chem.* **1983**, *22*, 50.

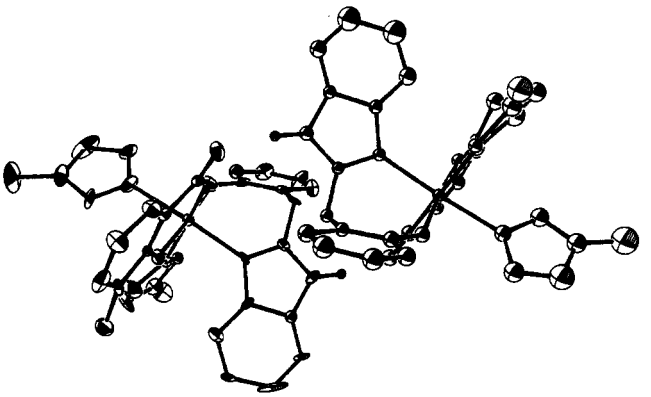

Figure 3. ORTEP diagram of the Fe(Bymp)(Msal)$(Mim)_2$ dimer. Note the orientation of the benzimidazole N–H bond toward the carboxylate oxygen of the neighboring monomer.

Table V. Charge-Transfer Spectral Data

compd	λ, nm[a]	ε, M^{-1} cm^{-1} [b]	compd	λ, nm[a]	ε, M^{-1} cm^{-1} [b]
1	524	2450	**7**	518	2250
2	513	2490	**8**	514	2120
3	529	1320	**9**	494	1450
4	476	1620	**10**	474	1340
5	460	860	**11**	460	690
6	500	1290			

[a] Spectra recorded in ethanol. [b] The bands are shoulders on the intense UV absorption, but the relative ε are unaffected by factoring out the UV tail.

of 129°. A similar case is observed for Fe(Salen)(Acac)[21] where the Fe–O–C bond angles are 136.1 and 128.3° and the phenolate oxygen-to-iron(III) bond lengths are 1.899 and 1.958 Å, respectively. The source of this difference in Fe(Salen)(Acac) appears to be a tetrahedrally distorted imine nitrogen in the Salen ligand, while in our case the observed differences arise from seven-membered ring puckering. The iron–imidazole bond lengths are 2.177 and 2.159 Å for the Fe–N1j and Fe–N1i bonds, respectively. Published values in this range suggest that these distances correspond well with those expected for a high-spin iron(III) environment.[24-26] The Fe–N9 bond length is 2.137 Å, and although it is an iron(III)–benzimidazole bond, it agrees well with those values observed for an iron–imidazole bond length in this particular spin state.

The molecule is organized into hydrophobic and hydrophilic regions. Part of the molecule appears quite hydrophobic, as the methyl groups C3iM, C3jM, and C3M are part of the ligands occupying one face of the octahedron. Opposite to this hydrophobic face of the octahedron is a region that appears more polar, with a cleft composed of oxygen atoms from O1a1, O1a2, and O1. This side of the molecule becomes involved in hydrogen bonding, as illustrated by Figure 3. The tendency toward strong H bonding of benzimidazoles in the solid state has been noted previously.[12,27,28] Hydrogen bonding, linking the benzimidazole NH and the carboxylate from N12 and O1a2 of one molecule to N12* and O1a2* of another molecule, leads to formation of a dimer. The distance between the hydrogen-bonded atoms N12 and O1a2* is 2.742 Å, while the Fe–Fe* distance is 7.984 Å. This

Table VI. Complex **10** in Different Donor Solvents at 25 °C

solvent	donor no.[a]	λ, nm	ε, M^{-1} cm^{-1}
piperidine	51.0	471	1730
pyridine	33.1	506	2680
dimethyl sulfoxide	29.8	497	2400
DMF	26.6	500	2550
formamide	24.0	480	2020
THF	20.0	474	1470
EtOH	20.0	474	1340
ethyl acetate	17.1	452	1000
acetone	17.0	460	1150
propylene carbonate	15.1	464	1280
acetonitrile	14.1	470	1330
benzonitrile	11.9	468	1250
nitromethane	2.7	464	1310

[a] Values from: Lever, A. B. P. *Inorganic Electronic Spectroscopy*; 2nd ed.; Elsevier: New York, 1984; p 211.

provides some further intrinsic interest to the structure of the model, but there is no evidence that the free energy of interaction between these two irons is similar to that for lactoferrin, wherein the two irons are 42 Å apart[9] (though covalently linked).

Electronic Spectra. The phenolate-to-iron(III) charge-transfer transition data for this series of complexes are in Table V. Diiron(III) lactoferrin (Fe_2Lf) has a very characteristic charge-transfer band at λ_{max} 465 nm (ε = 2070 L mol^{-1} cm^{-1} per iron). This charge transfer is assigned[8] to a transition from a p_π orbital on the tyrosinate oxygen to the half-filled d_{π^*} orbitals on the iron(III) ion. The complexes prepared for this study exhibit a range of λ_{max} from 460 to 529 nm and a range of molar absorptivities from 690 to 2490 L mol^{-1} cm^{-1}. Taking into consideration the differences in the ligands providing the phenolate coordination allows one to rationalize the observed wavelengths and molar absorptivities of the charge-transfer bands associated with each complex.

The data indicate that the larger molar absorptivities are observed with the complexes having two six-membered chelate ring systems (**1**, **2**, **7**, and **8**) as compared to the complexes with two seven-membered chelate ring systems (**5** and **11**), which have much lower molar absorptivities. Intermediate are the complexes that have both a six- and a seven-membered chelate rings (**3**, **4**, **6**, **9**, and **10**). As discussed above, the phenolate oxygens in the six-membered chelate rings have better overlap with the iron than those in the seven-membered chelate rings. The improved Fe–O overlap gives rise to the higher molar absorptivities observed for the complexes having two six-membered ring systems, while the opposite trend is observed in those complexes having a pair of seven-membered ring systems. The complexes containing an admixture of ring sizes of course have intermediate values.

It is not yet apparent from the protein crystallography that any stereochemical constraints are present in Fe_2Lf, so that the tyrosinates may well be less constrained than those in the bidentate chelate rings in these model complexes, where ring size affects restriction. Less constraint on the protein tyrosinates allows for better overlap, a situation mimicked by the complexes having two six-membered rings, as judged by the similarity in the values of the molar absorptivities.

The observed charge-transfer-band wavelength of Fe_2Lf closely correlates with the wavelengths of those complexes having a pair of seven-membered chelate ring model complexes. This is most likely a consequence of the incorporation of the methylene unit into the ligand structure, as it disrupts the conjugation between the phenolate ring and the benzimidazole rings and the carboxylate and the phenolate ring, thus increasing the energy of the charge-transfer transition. This particular situation is more akin to that in Fe_2Lf, where there is no conjugation between the amino acid side-chain donors.

However, no single model complex in this series is capable of mimicking both spectral features. The methylene unit creates a seven-membered ring, necessary for the disruption of conjugation, but leads to puckering, thus reducing the overlap of the phenolate oxygen with the iron. Therefore, the best model of the electronic

(22) Bertrand, J. A.; Breece, J. L.; Eller, P. G. *Inorg. Chem.* **1974**, *13*, 125.
(23) Sinn, E.; Sim, G.; Dose, E. V.; Tweedle, M. F.; Wilson, L. J. *J. Am. Chem. Soc.* **1978**, *100*, 3375.
(24) Kennedy, B. J.; McGrath, A. C.; Murray, K. S.; Skelton, B. W.; White, A. H. *Inorg. Chem.* **1987**, *26*, 483.
(25) Nishida, Y.; Kino, K.; Kida, S. *J. Chem. Soc., Dalton Trans.* **1987**, 1157.
(26) Tao, X.; Stephan, D. W.; Mascharak, P. K. *Inorg. Chem.* **1987**, *26*, 754.
(27) Addison, A. W.; Burke, P. J.; Henrick, K.; Rao, T. N.; Sinn, E. *Inorg. Chem.* **1983**, *22*, 3645.
(28) Sanni, S. B.; Behm, H. J.; Beurskens, P. T.; van Albada, G. A.; Reedijk, J.; Lenstra, A. T. H.; Addison, A. W.; Palaniandavar, M. *J. Chem. Soc., Dalton Trans.* **1988**, 1429.

Table VII. ESR Results in EtOH at 77 K

compd	g_2	g_4	g_4'	g_5	g_6	g_8	g_9	g_{10}
1		4.32			5.9	8.3		
2	2.03	4.35			5.7		8.7	10.2
3	2.05	4.38			5.7		8.8	
4	2.00	4.32						
5	2.04	4.35						
6	2.01	4.33	4.63	5.6	5.9	8.4	9.3	
7	2.00	4.34	4.50	5.5	5.9	8.3	9.2	10.1
8	2.02	4.34			5.7		9.0	10.2
9		4.32						
10		4.33						
11	2.05	4.38						

spectrum of Fe_2Lf is a composite of complexes **5** and **8**. Separately, both spectral features are successfully mimicked, with Fe–O overlap dictating molar absorptivity and donor type (phenolate for tyrosinate) dictating band wavelength. Furthermore, it becomes apparent that relatively small changes in geometry (and thus orbital overlap) may lead to differences in absorption spectra such as that observed between human lactoferrin and rabbit serum transferrin.

Solvent Effects. The two bidentate ligands occupy four of the coordination sites in the model complex, and solvent molecules fill the remaining two sites. A study of complex **10** in a variety of donor and nondonor solvents reveals a strong correlation of charge-transfer-band wavelength with solvent donor ability. Table VI is a compilation of the results of this study. Complex **10** was selected because the benzimidazole is N-methylated and should eliminate any complications associated with benzimidazole NH hydrogen-bonding donor ability.

Following the phenolate-to-iron(III) charge-transfer band as a function of solvent donor ability reveals a reasonable correlation ($r = 0.81$) between band wavelength and donor number. The data point for piperidine falls away from the correlation, presumably due to extensive displacement by this strong donor of other ligands coordinated to the iron(III).

Electron Spin Resonance. In frozen-ethanol glasses, this series of complexes exhibits spectral features typical of monomeric high-spin iron(III) in a rhombic ligand field and weakly coupled dimeric iron(III) complexes. The observed g factors for this series of complexes are found in Table VII. The resonances at $g = \sim 2.0$ arise from the dimerization of two high-spin monomeric complexes to produce a spin–spin-coupled dinuclear iron species.[6] The tendency of these complexes to hydrogen-bond and dimerize in the solid state has been noted previously (vide infra) and most of the complexes do exhibit some amount of association in ethanol solution at low temperature and in the solid state at room temperature. Monomeric iron(III) species in a rhombic ligand environment give rise to the intense signal at $g = 4.3$ and a weaker signal at low field, in the vicinity of $g = 8$. Complexes **1–3** and **6–8** all exhibit resonances at $g = 4.3$ and 8 in addition to one near $g = 5$. Complexes **6** and **7** show split sets of signals that probably arise from a mixture of isomers. Some of the complexes exhibit only an isotropic $g = 4.3$ signal, which ranges in intensity from strong (**4** and **9**) to weak (**5**, **10**, and **11**).

The neat powder spectra at room temperature and at 77 K typically exhibit a moderate to very strong resonance at $g = 2$ in addition to a pair of signals near $g = 4.0$ and 6.0. The Fe–Fe* distance of 7.984 Å (vide infra) separates the iron(III) atoms far enough apart to preclude any bonding interactions, and there are no simple atomic or molecular bridges connecting the iron atoms to provide a pathway for exchange. Therefore, in the solid state some of the iron(III) atoms are weakly coupled but others still give rise to ESR signals indicative of the presence of high-spin monomeric iron(III). The relative intensities of the resonances for monomeric and dimeric species vary from complex to complex. The spectra of complexes at room temperature and at 77 K differ only in the intensity of the high-field resonance, which decreases at low temperature due to depopulation of excited states.

The ESR spectra of a diferric transferrin and of ovotransferrin saturated with iron(III) consist of a three-component resonance, which is characteristic of iron(III) in a nonsymmetric ligand field and has a line shape expected for three unequal g values.[29] For diferric transferrin the solution spectrum has a three-component resonance at $g = 4.14$ and a low-field component at $g = 8.9$. Iron(III)–saturated ovotransferrin has its three-component resonance at $g = 4.12$, while on the low-field side of this signal there is a strong shoulder at $g = \sim 5$, and the low-field $g = 8.8$ signal is much stronger than the corresponding resonance in diferric transferrin.[30]

Obviously, very different iron environments exist among the synthetic complexes in solution, as evidenced by the variations in ESR signals observed. Even transferrin and ovotransferrin confer slightly different coordination environments on the iron(III), as determined by ESR spectroscopy (diferric lactoferrin has an ESR spectrum that is similar to diferric transferrin[31]). In general, the ESR parameters are quite sensitive to iron(III) coordination. The absence of a three-component resonace at $g = 4$ in the model complexes indicates that the active sites in the transferrins provide a unique environment not readily duplicated in synthetic models.

Cyanide Adducts. The report[32] of the characterization of a low-spin adduct of cyanide with C-terminal monoferric serum transferrin prompted us to examine the analogous reactions with the model complexes. On adduction, C-terminal monoferric serum transferrin exhibits a rhombic $S = {}^1/_2$ signal (the principal components are $g = 1.92$, 2.15, and 2.34), while N-terminal monoferric transferrin is not converted to the low-spin state, retaining its characteristic high-spin signal. Three cyanides are required to effect the spin-state change; therefore it is proposed that these three cyanides are coordinated to the iron(III), in addition to three of the original ligands. The cyanides presumably displace the (bi)carbonate and an amino acid side chain, although it is known that two of the three retained protein residues are the tyrosines.[33]

Spectrophotometric titration (ΔA vs $[CN^-]_{tot}$) of a solution of **1** with NaCN solution yields a breakpoint at 1.24 cyanides per iron; as these are presumably equilibrium processes, and also because this represents the maximum actual $Fe:CN^-$ ratio possible in this titration (because of the hygroscopic nature of solid NaCN), we take this to represent the 1:1 adduct. This has λ_{max} 450 nm and $\epsilon = 3200$ L mol^{-1} cm^{-1}, as estimated from this plot of normalized absorbance at 650 nm versus titrant added. The further addition of cyanide causes marked spectral changes; the adduct formed at a 1:2 $Fe:CN^-$ level has λ_{max} 655 nm ($\epsilon = 630$ L mol^{-1} cm^{-1}), and at the 1:3 level, λ_{max} 658 nm ($\epsilon = 1080$ L mol^{-1} cm^{-1}) is observed. The charge-transfer spectrum of **1** in absolute ethanol changes dramatically with the first few aliquots of cyanide solution; the phenolate-to-iron(III) charge-transfer band blue-shifts and the intensity increases. After 1:1 equivalence is attained, the band at about 655 nm appears and continues to grow with further addition of cyanide.

The ESR data for the adducts of cyanide and some of the model complexes are presented in Table VIII. Changes in the spectrum of **6** as a function of stoichiometric additions of cyanide are shown in Figure 4. The spectrum of the 1:1 adduct differs from the initial spectrum in a number of ways: (i) there is now a pair of low-spin $S = {}^1/_2$ iron(III) rhombic signals (the principal components are $g = 1.909$, 1.929, 2.206, and 2.418), presumably representing two different low-spin cyanide adducts; (ii) the high-spin iron(III) portion of the spectrum now appears to represent only one species (vide infra); (iii) the weak signal at $g = \sim 2.0$, indicative of the dimerization of two high-spin monomeric units, is absent, and the resonance at $g = 3.18$ (moderate intensity) is significantly weaker and has $g = 3.93$ in the spectrum of the 1:1 species; (iv) the addition of more cyanide (to the 1:2 level)

(29) Windle, J. J.; Wiersema, J. R. C.; Feeney, R. E. *Biochemistry* **1963**, *2*, 1341.
(30) Aasa, R.; Malmström, B. G.; Saltman, P.; Vänngård, T. *Biochim. Biophys. Acta* **1963**, *75*, 203.
(31) Ainscough, E. W.; Brodie, A. M.; Plowman, J. E.; Bloor, S. J.; Loehr, J. S.; Loehr, T. M. *Biochemistry* **1980**, *19*, 4072.
(32) Swope, S. K.; Chasteen, N. D.; Weber, K.; Harris, D. C. *Recl. Trav. Chim. Pays-Bas* **1987**, *106*, 259.
(33) Swope, S. K.; Chasteen, N. D.; Weber, K.; Harris, D. C. *J. Am. Chem. Soc.* **1988**, *110*, 3835.

Table VIII. ESR of Cyanide[a] Adducts in EtOH at 77 K

compd	g_2	g_2'	g_2''	g_4	g_4'	g_5	g_6	g_8	g_9
1				4.32			5.9	8.3	
1(CN)	1.904	2.206	2.418	4.35	4.63	5.3		8.4	9.2
1$(CN)_2$	1.909, 1.932	2.206	2.418	4.38	4.65	5.2			9.3
5				4.37					
5(CN)	1.909, 1.932	2.225	2.427	4.35					
5$(CN)_2$	1.941	2.193	2.340	4.37					
6				4.35	4.60	5.6	5.9	8.4	9.3
6(CN)	1.909, 1.929	2.206	2.418	4.38	4.60	5.1			9.5
6$(CN)_2$	1.909, 1.926	2.206	2.413	4.38		4.9			9.5
6$(CN)_3$	1.912, 1.926	2.206	2.413	4.38	4.55	5.0			9.5
10				4.33					
10(CN)	1.86	2.222	2.441	4.32					
10$(CN)_2$	1.929	2.183	2.332	4.32					9.3

[a] Cyanide ion added as NaCN in absolute EtOH.

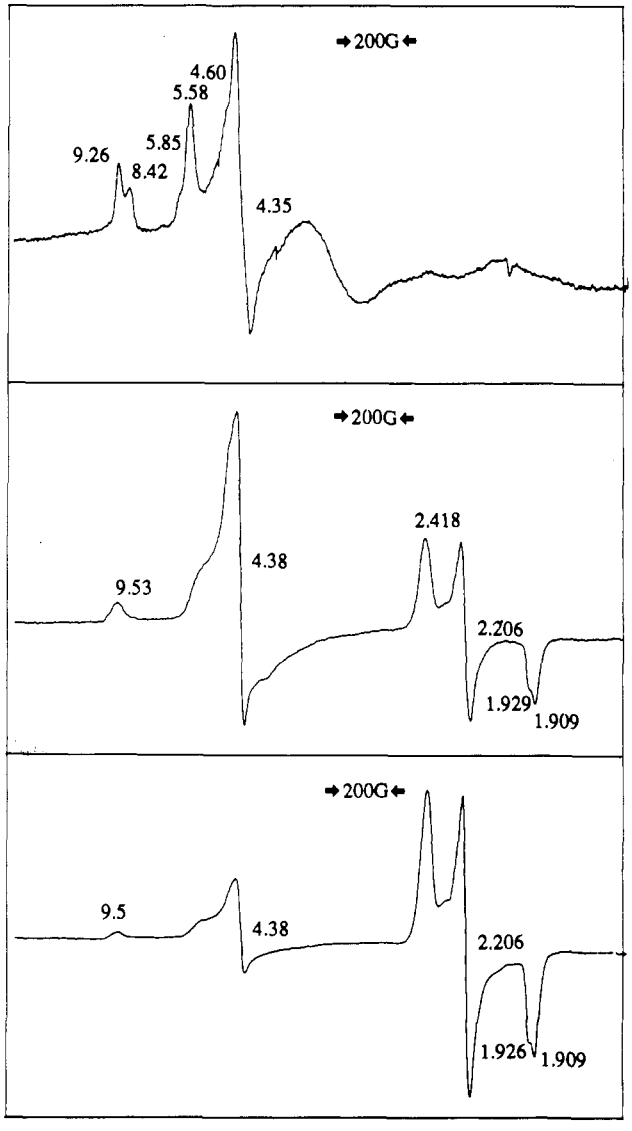

Figure 4. ESR spectra of complex **6**, Fe(Bp)(Hpa)·$2H_2O$, in EtOH at 77 K: (upper) 14 mM **6** in the absence of cyanide; (center) 19 mM each of **6** and NaCN; (lower) 12 mM of **6** plus 25 mM NaCN.

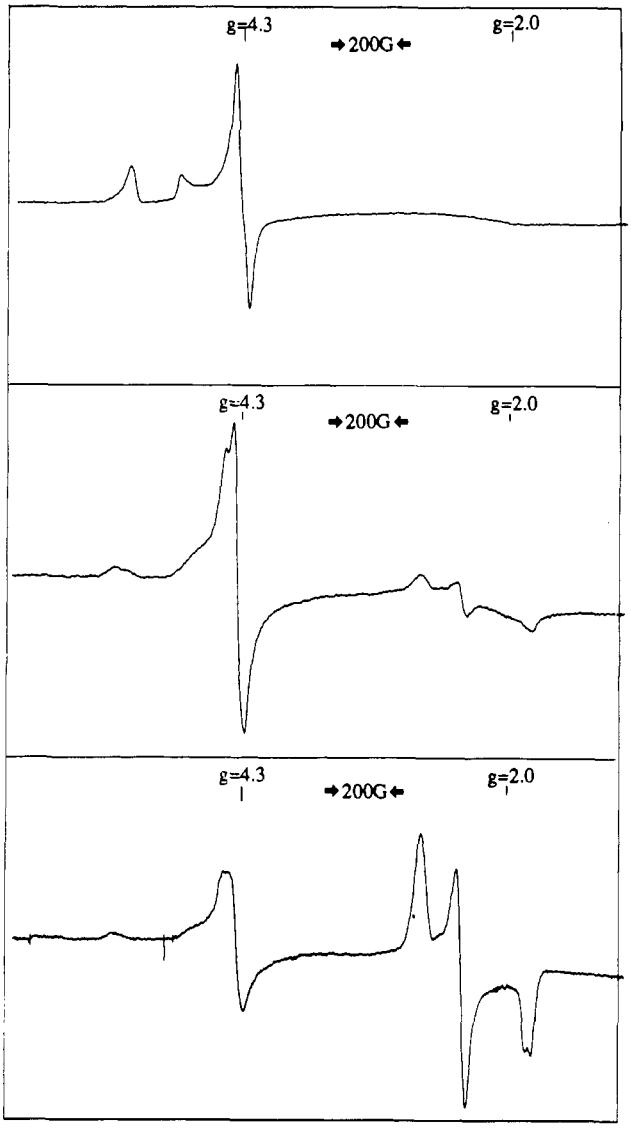

Figure 5. ESR spectra of complex **1**, Fe(Bp)(Sal)·$4.25H_2O$, in EtOH at 77 K: (upper) 49 mM **1** in the absence of cyanide; (center) 38 mM **1** plus 38 mM NaCN; (lower) 24 mM **1** plus 48 mM NaCN.

increases the amount of the low-spin species relative to the high-spin species.

Figure 5 illustrates the ESR results for the stepwise adduct formation of cyanide with complex **1**, which is a simpler situation than the above, in that **1** appears to consist of only one high-spin component with little dimer formation. Further comparisons with the data in Figure 4 demonstrate the following: (i) the 1:1 spectrum of **1** shows the formation of the same rhombic low-spin iron(III) species as in Figure 4 (the principal components are g = 1.904, 2.206, and 2.418), yet the intensity of these resonances is less in comparison to the high-spin component than in the case of **6**; (ii) the 1:1 high-spin component in Figure 5 is similar to that in Figure 4; (iii) complex **1** and its cyanide adducts have no resonances at $g = 3$; (iv) the further addition of cyanide (to the 1:2 level) greatly enhances the signal of the low-spin species relative to the high-spin species, and the high-field resonance resolves clearly into *two* low-spin iron(III)–cyanide adducts (the principal components are g = 1.909, 1.932, 2.2068 and 2.418).

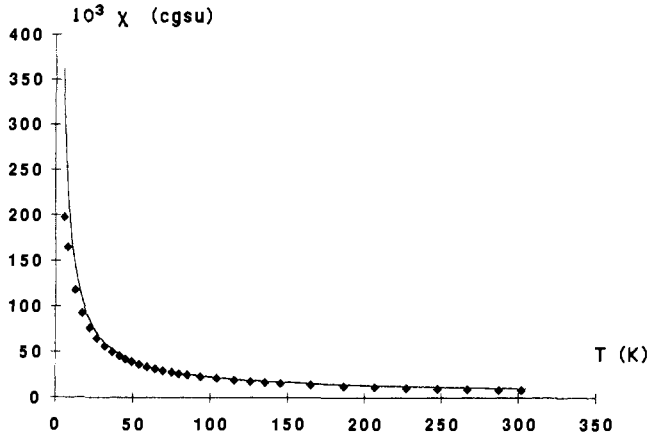

Figure 6. Magnetic susceptibility data for compound **6**, Fe(Bp)(Hpa)·$2H_2O$. The points correspond to the experimental data, the line to the calculated fit model.

The behavior of both **1** and **6** must be considered together in order for an interpretation of the observed spectra of the cyanide adducts to be made. Compound **6** appears to be a mixture of two slightly different (via the ESR criterion) monomeric complexes (perhaps geometric isomers) in equilibrium, in addition to some dimeric species, while **1** appears to be a single species. The stepwise addition of cyanide causes two ESR features to change: first, any dimeric species present are presumably separated into monomeric complexes, and second, the adduct formed between cyanide and some portion of the complexes in solution gives rise to a pair of low-spin iron(III) signals while some portion of the complexes remain as high-spin iron(III) in solution.

The addition of cyanide to C-terminal monoferric transferrin disrupts its unique structure and causes the ESR spectrum to change in such a manner as to resemble that of the cyanide adducts of the model complexes. The change in the absorption spectrum upon cyanide coordination in the protein also resembles the change observed in the model complexes. The charge-transfer band is blue-shifted from 460 to 420 nm when cyanide is coordinated to the C-terminal site,[33] which is similar to the initial spectral changes observed during the formation of the 1:1 cyanide adduct of **1**. Further cyanide addition to the model compounds appears to cause a red shift, while bis-adduction by *N*-methylimidazole clearly red-shifts the absorption; however, the parent compounds and the 1:1 adducts do not necessarily have the same (trans) stereochemical relationship between these two phenolate CT donors as does the bis(*N*-methylimidazole) adduct (see comment concerning possible isomers of **6**). Note that, in the protein, equilibrium redistribution of ligands over irons in solution cannot occur, as they are fixed in place relative to just one iron.

Magnetism. Because the ESR spectrum of **6** showed evidence for Fe–Fe interactions, its magnetic susceptibility was determined over the temperature range 5.6–301.8 K. The effective magnetic moment, μ_{eff}, at room temperature is 4.5 μ_B, significantly less than the spin-only value (5.9 μ_B) for $S = {}^5/_2$ iron(III). The ESR spectrum of compound **6**, shown in Figure 4, has resonances at $g = 3$ and 2, which are assignable to weakly coupled high-spin monomeric iron(III) species, consonant with the H-bonded dimerization observed in the X-ray crystal structure of its adduct, Fe(Bymp)(Msal)$(Mim)_2$. The value of μ_{eff} for **6** decreases with decreasing temperature, indicating an antiferromagnetically coupled system.

Generation of a χ^M versus temperature curve allows one to fit[20] the experimental data and deduce values for the magnetic exchange integral, J, the percent paramagnet content, and the temperature-independent paramagnetism, TIP.[34] The best fit for this compound is with the majority of the iron(III) ions present in a moderately antiferromagnetically coupled form ($-2J = 40$ cm^{-1}; 60%) and the rest as mononuclear (or at least noncoupled) molecules. This is associated with g close to the free-electron value, $10D_q = 10400$ cm^{-1} and TIP = 200×10^{-6} emu mol^{-1} (to which values the fit is relatively insensitive). The $-2J$ value is rather larger than is observed for a doubly bridged iron(III) complex (0 to -10 cm^{-1}) yet considerably lower than would be indicative of strongly coupled Fe–O–Fe units (ca. -200 cm^{-1}).[35] The ligation of **6** is such that the magnetic exchange may arise from carboxylate bridging between the iron(III) atoms, leading to stronger coupling than would be expected just for H-bonded dimerization.[12,27,28] We appreciate that the solid-state composition may simply represent the net solubility of such a dimerizing system at equilibrium.

Electrochemistry. These complexes exhibit non-Nernstian behavior in the nonaqueous solvents examined. Complex **6** was characterized in more detail in TEAP/DMF at a planar Hg electrode by using rotating-disk polarography and cyclic voltammetry. The $E_{1/2}$ value is -1360 mV versus the $Ag/AgClO_4$ reference electrode (ca. -815 mV versus the SHE), and an n value of 1.04 was obtained from an iR-corrected plot of the rde polarographic log $((i_{LIM} - i)/i)$ vs E data for the irreversible charge-tranfer case.[36] The value of n was calculated by using $\alpha = 0.81$, determined from the form of the Randles–Sevcik equation appropriate to an irreversible charge transfer[37] using cyclic voltammetry data. In order to use this method for determination of α, the diffusion coefficient was calculated from a double-reciprocal plot of the limiting current versus the square root of rotation rate for the case of an irreversible charge transfer[38] using rde data, as this current function is independent of α. The associated value of D is 3.4×10^{-6} cm^2 s^{-1}, and $D\eta$ is 2.9×10^{-8} g cm s^{-2}, which in turn is internally consistent with $n = 1$.

Four different estimates for $E^{\circ\prime}$ of iron transferrin have been reported.[10,39-41] The Fe(II)- and Fe(III)–transferrin binding constants yield a calculated value of $E^{\circ\prime} = -140$ mV for diferric transferrin.[39] Reduction of diferric transferrin using the dithionite ion ($E^{\circ\prime} = -527$ mV) has been effected, within the recognition that the reductive release of iron from the protein depends, among other things, on pH, the nature of the reducing agent, the presence of chelating agents, and synergistic anion-binding effects.[40] The reduction potential has been measured spectrophotometrically,[41] and it was observed that half of the iron(III) is reduced at a potential near -400 mV vs the SHE, while at high ionic strength differic transferrin is reported to have $E^{\circ\prime} = -520$ mV versus the SHE.[10] Since most biological reducing agents have $E^{\circ\prime}$ more positive than -320 mV, if iron is released via a reductive process, then clearly there must be factors operating other than a simple electron transfer to effect any release of transferrin iron in vivo.[10,40]

The value of -815 mV for complex **6** in TEAP/DMF is comparably low but is significantly more negative than those reported for diferric transferrin itself. This difference is presumably a consequence of such factors as variances in the dielectric constant of the solvent medium vs the protein active site[42] and the substitution of DMF solvent molecules in the model experiment by (bi)carbonate ion in the active site of the protein. In the case of diiron(III) transferrin the active site is postulated to be quite hydrophilic.[9] Note that the iron(III) model complex is neutral, while reduction places an overall -1 charge on it, so that, in a medium of lower effective mean polarity than the protein active site, the iron(II) form is less stabilized, leading the reduction to occur at more negative potentials.

(34) Mukerjee, R. N.; Stack, T. D. P.; Holm, R. H. *J. Am. Chem. Soc.* **1988**, *110*, 1850.
(35) Cotton, F. A.; Wilkinson, G. *Advanced Inorganic Chemistry*; John Wiley & Sons: New York, 1980; p 761.
(36) Sawyer, D. T.; Roberts, J. L., Jr. *Experimental Electrochemistry for Chemists*; John Wiley & Sons: New York, 1974; p 337.
(37) Bard, A. J.; Faulkner, L. F. *Electrochemical Methods*; John Wiley & Sons: New York, 1980; p 222.
(38) Piekarski, S.; Adams, R. N. In *Techniques of Chemistry*; Weissberger, A., Rossiter, B. W., Eds.; John Wiley & Sons: New York, 1971; Vol. I, Part IIA, p 571.
(39) Harris, W. R. *Biochemistry* **1983**, *22*, 3920.
(40) Kojima, N.; Bates, G. W. *J. Biol. Chem.* **1979**, *254*, 8847.
(41) Harris, D. C.; Rinehart, A. L.; Herald, D.; Schwartz, R. W.; Burke, F. P.; Salvador, A. P. *Biochim. Biophys. Acta* **1985**, *838*, 295.
(42) Ru, Y.; McDevitt, M. R.; Addison, A. W. *Abstracts*, XXVIIth International Conference on Coordination Chemistry, Brisbane, Australia, 1989; W54.

Conclusions

The solution chemistry of iron(III) having a set of ligands similar to those provided by lactoferrin is analogous to the chemistry of iron(III) in the transferrins with regard to reactivity, spectroscopic, and electrochemical considerations. It is unclear as to whether the model systems or the proteins represent more structurally constrained situations with respect to the iron(III) coordination geometry, though the protein active sites appear to be more rhombically distorted than the models, as judged by the three g values observed in the high-spin ESR spectrum of the diiron(III) proteins. The cyanide adducts of the model compounds closely resemble the low-spin cyanide adduct of transferrin, illustrating the susceptibility of at least one of the two iron(III) sites to cyanide adduction and the subsequent disruption of its "native" coordination. The wavelength and molar absorptivity of the tyrosinate-to-iron(III) charge-transfer band are individually mimicked by the substituted bidentate phenolate ligands, demonstrating the utility of using ligands isostructural with amino acid residues. The quite negative redox potential of diferric transferrin precludes simple noncooperative reduction via endogenous reducing agents in vivo. The irreversible electrochemical reduction of the model complexes at quite negative potentials is related to the intrinsic stability of these iron(III) complexes with this given set of ligands and reiterates the stability of the iron(III) atom in the lactoferrin active site.

Acknowledgment. We thank Drexel University for support.

Supplementary Material Available: Listings of anisotropic thermal parameters, additional bond angles, and least-squares planes (9 pages); a table of observed and calculated structure factors (17 pages). Ordering information is given on any current masthead page.

Contribution from the Department of Chemistry, Carnegie Mellon University, 4400 Fifth Avenue, Pittsburgh, Pennsylvania 15213

Chromium(V)–Oxo Complexes of Macrocyclic Tetraamido-*N* Ligands Tailored for Highly Oxidized Middle Transition Metal Complexes: A New ^{18}O-Labeling Reagent and a Structure with Four Nonplanar Amides

Terrence J. Collins,*[1a] Carla Slebodnick, and Erich S. Uffelman[1b]

Received March 22, 1990

Two chromium(V)–oxo complexes, $[(CH_3)_4N][Cr(O)(\eta^4\text{-}\mathbf{1})]$ and $[(CH_3)_4N][Cr(O)(\eta^4\text{-}\mathbf{2})]$, have been synthesized and characterized by X-ray crystallography and IR and EPR spectroscopies. Because exchange of the oxo ligand with water is slow, the easily synthesized, stable, crystalline ^{18}O-labeled diperoxide $(CH_3)_2(H^{18}O^{18}O)CCH_2CH_2C(^{18}O^{18}OH)(CH_3)_2$ was prepared and used to conveniently synthesize ^{18}O-labeled oxo complexes in high yields. The bonding of the two unique oxidation-resistant macrocyclic tetraamides to chromium is compared. The structural and EPR properties are consistent with a chromium-centered radical in each case and suggest that a chromium(V) oxidation state assignment is equally appropriate whether the ancillary ligand is the innocent $[\eta^4\text{-}\mathbf{1}]^{4-}$ or the potentially noninnocent $[\eta^4\text{-}\mathbf{2}]^{4-}$. Both oxo complexes contain nonplanar amide groups. The distortions in $[Cr(O)(\eta^4\text{-}\mathbf{1})]^-$ are more marked, and it is a unique species in containing four distinctly nonplanar amides. The discovery of these unusual structural parameters expands the class of nonplanar amides arising from ring constraint.

Introduction

The scarcity of highly oxidized middle and later transition metal complexes[2] challenges chemists to develop ligand complements compatible with oxidizing metal centers. An objective of our program in this area[3a] is to understand how the structural and electronic properties of specifically designed ancillary ligand complements affect the properties of new metal–oxo species. One aspect of this interrelationship arises when one wishes to contribute new species to the very small class of highly oxidized middle and later first row transition metal complexes. In such cases it is important to consider the possibility of ligand noninnocence, the ability of a ligand to become part or all of the redox-active site of the complex. Here we describe two unique macrocyclic tetraamido-*N* ligands, the innocent H_4-**1** and potentially noninnocent H_4-**2**,[3b] where the dichlorophenylenediamide unit is a possible site of oxidation in highly oxidized complexes. We have examined these ligands, which are remarkably resistant to oxidative decomposition, by comparing the chromium(V)–oxo complexes. Although there are significant differences in the structures of the two ligands, the relevant structural properties and the EPR spectra of the five-coordinate monoanionic chromium(V)–oxo complexes indicate that the assignment of the +V oxidation state to the chromium center is equally appropriate in both cases. In addition,

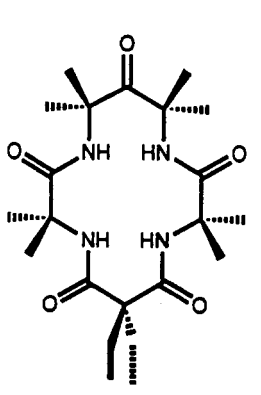

H_4-**1**

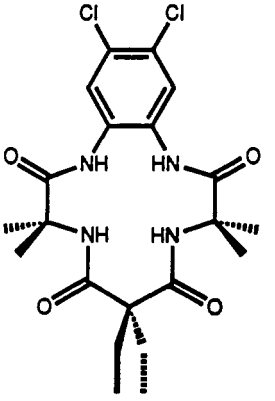

H_4-**2**

(1) (a) Dreyfus Teacher-Scholar, 1986–1990; Alfred P. Sloan Research Fellow, 1986–1989. (b) California Institute of Technology. Current address: Department of Chemistry, Carnegie Mellon University.

(2) For comprehensive discussions, see: (a) Nugent, W. A.; Mayer, J. M. *Metal-Ligand Multiple Bonds*; Wiley-Interscience: New York, 1988. (b) Holm, R. H. *Chem. Rev.* **1987**, *87*, 1401–1449. (c) Sheldon, R. A.; Kochi, J. K. *Metal Catalyzed Oxidations of Organic Compounds*; Academic Press: New York, 1981. For a review of chromium(V) coordination chemistry see: (d) Mitewa, M.; Bontchev, P. R. *Coord. Chem. Rev.* **1985**, *61*, 241–272.

(3) (a) For initial reference, see: Anson, F. C.; Christie, J. A.; Collins, T. J.; Coots, R. J.; Furutani, J. J.; Gipson, S. L.; Keech, J. T.; Krafft, T. E.; Santarsiero, B. D.; Spies, G. H. *J. Am. Chem. Soc.* **1984**, *106*, 4460–4472. (b) For a discussion of the terms "innocent" and "noninnocent", see: Anson, F. C.; Collins, T. J.; Richmond, T. G.; Santarsiero, B. D.; Toth, J. E.; Treco, B. G. R. T. *J. Am. Chem. Soc.* **1987**, *109*, 2974–2979.

0020-1669/90/1329-3433$02.50/0